RSC Advances

PAPER

View Article Online
View Journal | View Issue

Cite this: *RSC Adv.*, 2024, **14**, 39325

In vivo and *in silico* evaluation of the phytoalexin-eliciting activity in common bean (*Phaseolus vulgaris* L.) of jasmonoyl-L-isoleucine analogs having a pyrazolidin-3-one ring†

Samuel Vizcaíno Páez, [ab] Diego Durango [b] and Wiston Quiñones *[a]

Jasmonates are phytohormones derived from jasmonic acid that regulate metabolic processes involved in the chemical response of plants to biotic and abiotic stress. As part of this response, some species synthesize *de novo* compounds with biological activity against some pathogens. In this work, nine analogs of jasmonoyl-L-isoleucine containing a pyrazolidin-3-one core were tested in their activity to elicit the production of phytoalexins (daidzein, genistein, coumestrol, and phaseollin) in common bean (*Phaseolus vulgaris* L.) cultivars when added exogenously. Some variations in selected parts of the analogs, such as the side chain, the linker, or the conjugated amino acid, allowed the establishment of qualitative relations with the observed activity. The analogs were tested at two levels of concentration, and the observed activity was, in most cases, higher than the observed for methyl jasmonate at 0.5 mM, even at the lower level. Seedlings treated with most heterocyclic compounds exhibited significantly higher amounts of phaseollin than untreated seedlings. Jasmonoyl-L-isoleucine analogs having a pyrazolidin-3-one ring trigger the production of phytoalexins and can be used for crop protection. Additionally, the protein-complex receptor involved in the jasmonate signaling mechanism was modeled by homology for *P. vulgaris*, using that for *Arabidopsis thaliana* as a template. After being modeled, it was assessed and used to qualitatively correlate the observed activity values and the vina scores from the docking of the tested analogs.

Received 7th September 2024
Accepted 29th November 2024

DOI: 10.1039/d4ra06461e

rsc.li/rsc-advances

1 Introduction

Jasmonates are a group of lipid-derived signalling ubiquitous phytohormones, including jasmonic acid (JA) and its derivatives (*e.g.* methyl jasmonate, MeJA; certain amino acid conjugates like jasmonoyl-L-isoleucine, JA-Ile; decarboxylated forms; glucose esters and hydroxylated forms). The JA-Ile has been reported to be the bioactive form of jasmonates in plants, as it acts as a ligand for the jasmonate receptor (the F-box protein CORONATINE INSENSITIVE 1 (COI1) and repressor protein JASMONATE ZIM-DOMAIN (JAZ) to form the COI1-JAZ co-receptor system).[1] Jasmonates are known to be involved in different physiological mechanisms and metabolic pathways, and specially, the activation of a number of induced defensive responses in a wide array of different plant species.[2,3] Compounds with this activity are called elicitors, and many have been commercially released in some countries as plant health promoters for use in crops (*e.g.* the chemical inducer benzo (1,2,3)-thiadiazole-7-carbothioic acid-*S*-methyl ester or ASM or Bion® or Actigard®). Since jasmonates are responsible for the activation of defensive responses against different biotic stresses including pests and diseases in plants, it was suggested that exogenous application of jasmonates could be an efficient alternative to chemical agents that act through biocidal mechanisms in food production systems.[2] Several studies have shown that foliar spraying of plants and post-harvest treatment of harvested crops with jasmonates effectively improve the resistance mechanisms of the plant and the harvested crops.[2] MeJA, the most widely studied and most commercially available jasmonate, has also been evaluated as a successful plant protection treatment in several pathogen- and pest insect systems.[2] Unfortunately, exogenous application of MeJA in crop protection presents some challenges, due to its low water solubility, high volatility, strong and persistent odor, and because it can generate some phytotoxicity symptoms.[4] Furthermore, since the cyclic structure (a disubstituted cyclopentanone) of jasmonates (MeJA, JA, and JA-Ile) has two chiral carbons, only certain configurations have been found to be active. Furthermore, since the cyclic structure (a disubstituted cyclopentanone) of jasmonates (MeJA, JA, and JA-Ile) has two

[a]*Química Orgánica de Productos Naturales, Universidad de Antioquia, Medellín, 050010, Antioquia, Colombia. E-mail: wiston.quinones@udea.edu.co*

[b]*Química de los Productos Naturales y los Alimentos, Universidad Nacional de Colombia, Medellín, 050034, Antioquia, Colombia*

† Electronic supplementary information (ESI) available. See DOI: https://doi.org/10.1039/d4ra06461e

chiral carbons, only certain configurations have been found to be active.[5,6] This fact further limits the possible application of jasmonates in the field, since the synthesis and purification of the active stereoisomer can be complex and not commercially viable.

On the other hand, common bean (*Phaseolus vulgaris* L., Fabaceae), is the most commonly consumed legume worldwide for its edible dry seeds or green, unripe pods. In fact, it is the most important legume produced for direct human consumption with a commercial value greater than that of all other leguminous crops combined. However, common bean is susceptible to many pests and diseases which significantly affect crop yield. Traditionally, the use of biocidal chemical agents (insecticides, fungicides, *etc.*) has been the primary approach to address these factors. New insect pest and disease control agents that act through more environmentally friendly mechanisms are needed. One such approach is the stimulation of the natural intrinsic mechanisms that plants possess to counteract the attack of insects and pathogenic microorganisms.

Chemical defenses in plants involve induced secondary metabolites (called phytoalexins) and preformed ones (called phytoanticipins). Phytoalexins have been defined as antimicrobial compounds produced by plant tissues in response to microbial infection.[7,8]

In the case of leguminous plants such as *P. vulgaris*, these molecules belong to the isoflavonoid family, subgroups isoflavones, isoflavanones, isoflavans, coumestans, and pterocarpans, whose biosynthetic routes are described in Fig. 1. According to this, the known chalcone biosynthesis is the starting point, placing the narigenin chalcone (**1**) as common precursor. At this point, ring-closing and aryl migration lead to the corresponding isoflavone, but the hydroxylation in position 6′ or the lack of it, branches the route to the isoflavones daidzein (**2**) or genistein (**3**). From **2**, another hydroxylation in the new 6′ position is a requirement to form the five-membered ring of the coumestan coumestrol (**4**) or the pterocarpan phaseollin (**5**). All these compounds have been isolated and tested for their biological activity. For instance, Van Etten *et al.*[11] isolated phaseollin, kievitone, phaseollidin, and phaseollinisoflavan from hypocotyls of *P. vulgaris* infected with *Rhizoctonia solani*, and the ED_{50} for the inhibition of the radial growth of *R. solani* in solid media poisoned with these phytoalexins were 18, 36, 20 and 27 μg mL^{-1} respectively. These authors also examined the mode of action of phaseollin in *R. solani*, concluding that this should act on the plasmatic membrane or affect some processes needed for membrane functions.[12] Coumestrol, genistein, and daidzein isolated from infected young twigs of *Erythrina crista galli* showed antimicrobial activity against *Bacillus brevis* with MIC values in the μM range.[13] Genistein is also associated with the effective development of root nodules.[14]

The induction of phytoalexin production in *P. vulgaris* has been tested with amino-sugars,[15] analogs of salicylic acid,[9] derivatives of indanone with alkyl and amino acidic side chains,[16–19] most of them compared to the activity of methyl jasmonate (**6**). However, no jasmonate analogs have been tested in this species. Structures containing pyrazolidin-3-one core,

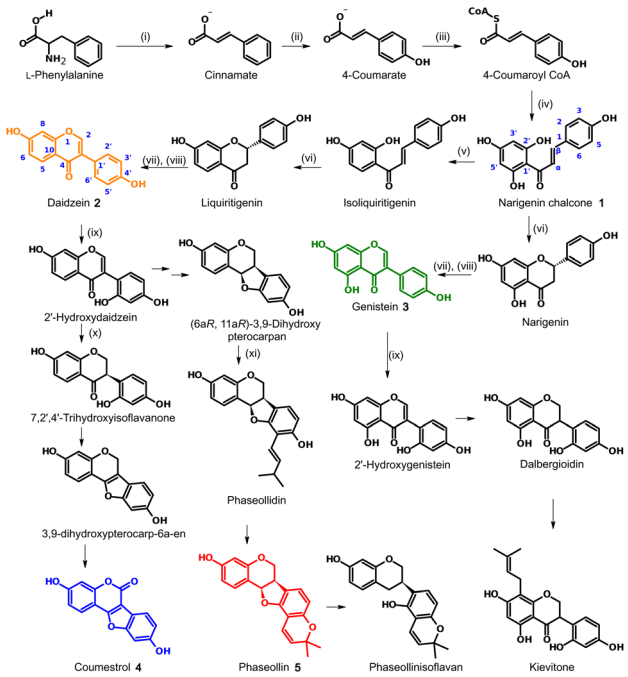

Fig. 1 Biosynthetic pathway of the main phytoalexins in *Phaseolus vulgaris*.[9,10] Enzymes: (i) phenylalanine ammonia-lyase (PAL); (ii) cinnamate 4-hydroxylase (C4H); (iii) 4-coumaroyl CoA ligase (4CL); (iv) chalcone synthase (CHS); (v) chalcone reductase (CHR); (vi) chalcone isomerase (CHI); (vii) isoflavone synthase (IFS); (viii) 2-hydroxyflavanone dehydratase (HID); (ix) isoflavone 2′-hydroxylase (IFH); (x) isoflavone reductase (IFR); (xi) prenyl transferase (PT).

similar to the synthesized analogs **7a–i** (Fig. 2), have been reported as a potent and selective agonist of Prostaglandin E_2 (PGE_2), a group of mammal hormone-like compounds with

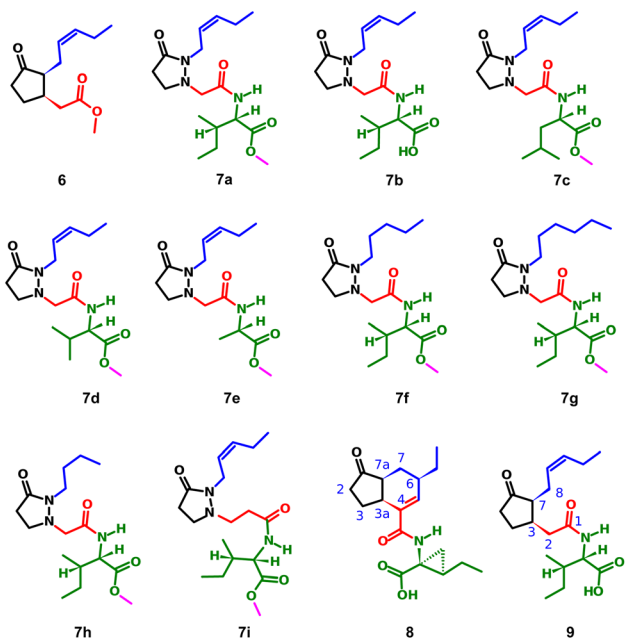

Fig. 2 Structure of methyl jasmonate (**6**), the tested compounds (**7a–i**), coronatine (**8**) and (+)-7-iso-jasmonoyl-L-isoleucine (**9**).

similar biosynthetic origin as jasmonates in plants. The molecular target of jasmonates has been devised since 2009 by homology with auxin mechanism, and taking advantage of the potent activity of the phytotoxin coronatine (COR, **8**) (a super strong jasmonate mimetic produced by *Pseudomonas syringae*) as an agonist of jasmonates, the (+)-7-iso-jasmonoyl-L-isoleucine (**9**) could be addressed as the main endogenous bioactive jasmonate.[1] Finally, in 2010, the protein complex of COronatine-Insensitive 1 (COI1) and the degron of JAsmonate Zim-domain (JAZ) was co-crystallized with both **8** and **9** by Sheard *et al.*,[20] enabling the study of molecular interactions through computational approaches such as docking or molecular dynamics.[21] To understand the molecular interactions between jasmonates and structurally related compounds and the COI1-JAZ co-receptor in bean, a 3D model of the protein complex is demanded. In addition, a molecular modelling could be used to identify potential elicitors in common bean and may be helpful to explain the experimental results. In this work, we present the test of jasmonate analogs containing a pyrazolidin-3-one ring as potential elicitors of phytoalexin production in a specific variety of *P. vulgaris*, along with the construction and evaluation of the corresponding protein-complex target in the common bean by homology to that reported for *Arabidopsis thaliana*, and its use as jasmonate receptor for docking screening.

2 Results and discussion

2.1 Phytoalexin-eliciting activity of the pyrazolidin-3-one analogs in *P. vulgaris*

Fig. 3 top displays the quantification of the elicited phytoalexins as the mean of the two replicas and the standard deviations as the vertical error bars.

With the solutions of the analogs set at 0.05 mM, the levels of isoflavones **2** and **3** were relatively low, **7e** being the one with the highest production. However, these amounts do not exceed 2.2 μg g^{-1} f.w. for **2** or 0.4 μg g^{-1} f.w. for **3**. According to our previous observations in time course experiments, the amount of the precursors tends to decrease after the first 24 hours as the plant produces pterocarpans, coumestans, or their prenyl derivatives in the corresponding biosynthetic route.[16] The amounts of pterocarpan and coumestan were comparatively higher than that of isoflavones at this time of post-induction, reaching values of 5.1 μg g^{-1} f.w. for **4** when induced with **7b** and 33.6 μg g^{-1} f.w. for **5** when **7e** was the inductor.

Treatments without elicitors (-blank) were employed as witnesses to compare the base levels of phytoalexins in the seedlings. These were set to the same conditions but using 0.5% EtOH solution instead of the potential elicitor. This way, a base amount of coumestan and pterocarpan was observed, yielding 2.4 μg g^{-1} f.w. of **4** and 6.7 μg g^{-1} f.w. of **5**. These values constitute a baseline for these compounds, demonstrating that the chosen variety of *P. vulgaris* (ICA Quimbaya) was sensitive enough to the unavoidable stress conditions of the experiment.

In general, the amount of phytoalexins in common bean seedlings treated with methyl jasmonate and the heterocyclic analogs of JA-Ile was dependent on the concentration of the

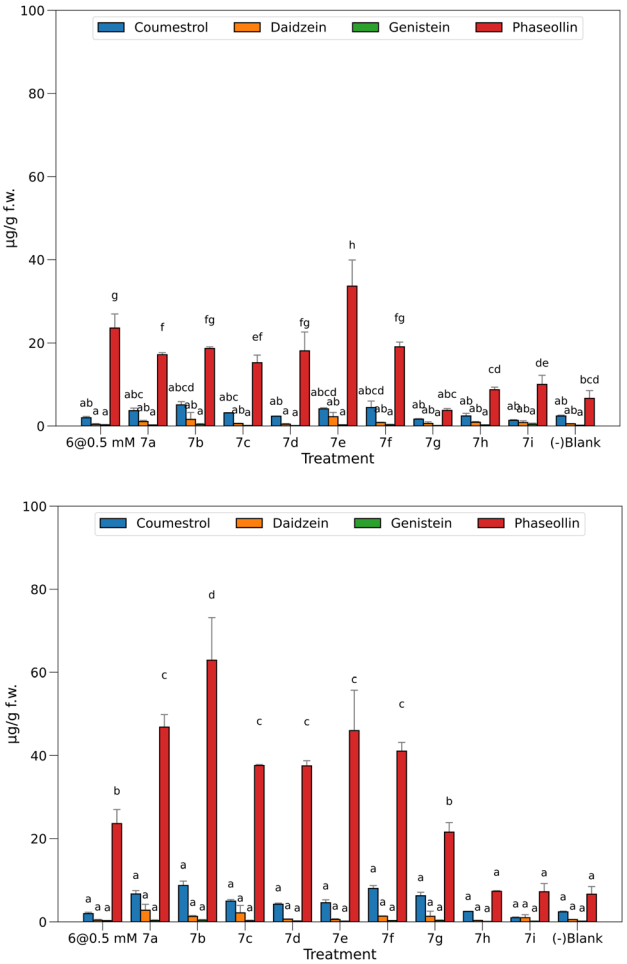

Fig. 3 Phytoalexins from *P. vulgaris* produced by the treatments at 0.05 mM (top) and 0.5 mM (bottom). Bars sharing the same letter has no significant differences.

potential elicitor. With the solutions of the heterocyclic analogs set at 0.05 mM, the levels of the isoflavones **2** and **3** were relatively low, and did not exceed 2.2 μg g^{-1} f.w. for **2** or 0.4 μg g^{-1} f.w. for **3**. The amounts of pterocarpan and coumestan were comparatively higher than that of isoflavones at this time of post induction, reaching values of 5.1 μg g^{-1} f.w. for **4** when induced with **7b** and 33.6 μg g^{-1} f.w. for **5** when **7e** was the inductor. These findings are consistent with previous research on elicitation in common bean in time course experiments, when the amount of the precursor isoflavone tends to decrease after the first 24 hours as the plant produces pterocarpans, coumestan, or their prenyl derivatives in the corresponding biosynthetic route. It was reported that the difference in chemical response to diseases between susceptible and resistant common bean varieties does not lie in the concentration of precursors, but is more marked in the later stages of the biosynthetic pathway. Thus, it was proposed that phaseollin may be a chemical indicator of resistance in common bean. It has also been suggested that susceptibility in common bean to pathogenic microorganisms may be associated with failures and delays in the prenylation process, which leads to the formation of the phytoalexins phaseollin and kievitone. Methyl

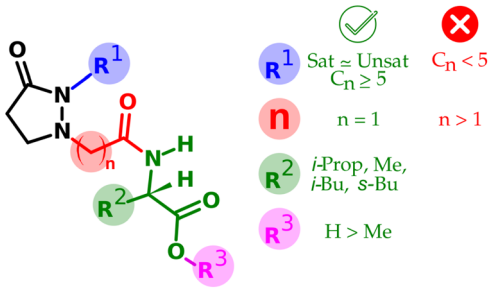

Fig. 4 Summary of the SAR observed for the tested compounds.

jasmonate (**6**) is a well-known elicitor of this kind of activity, a fact that was also seen in this bioassay because treatment with solutions at 0.5 mM does elicit biosynthesis of **5** up to 23.6 μg g^{-1} f.w., more than in untreated plants (-blank). However, it was not higher than that in **7e**. Considering the significant differences between the means, a group of three treatments did not surpass the baseline (**7g–i**), while the other six induced the biosynthesis of **5** in a ratio of 2.3 to 5 times more than in the untreated ones.

Interestingly, concentration of **5** was significantly higher in common bean seedlings treated with **7e** at 0.05 mM than with methyl jasmonate.

Fig. 3 bottom shows the results for the quantified amounts of phytoalexins after inducing with elicitors at 0.5 mM.

The higher levels of **4** and **5** compared with precursor **2** indicate a high efficiency in conversion to more advanced stages in the biosynthesis as a result of the treatments. Regarding **4** and **5**, most of the tested elicitors showed a dose-dependent behavior, excepting **7h** and **7i**, which were also inactive at 0.05 mM. In a second group, **7g** was inactive at 0.05 mM, but the increment in concentration induced the production of **5** at a similar amount (21.5 μg g^{-1} f.w.) than for the well-known elicitor **6** (23.6 μg g^{-1} f.w.). Surprisingly, the rest of the heterocyclic jasmonoyl analogs are in a third group, yielding **5** in ratios of 5.6 to 7 times the value of the untreated seedlings (-blank), and from 1.6 to 2.7 times than with the elicitor **6**. Interestingly, the free acid **7b** produced the highest amount of **5** at this concentration, 62.9 μg g^{-1} f.w., representing almost ten times more than in the negative blank.

A direct comparison of **7b** with **7a** reveals a 34% increment when the carboxylic group is unprotected. However, a more comprehensive analysis of the relation between the structural features and the observed activity is addressed in Fig. 4.

A fact to be considered is that the routes toward the coumestan **4** and the pterocarpan **5** come from the same precursor **2**, but the tested elicitors selectively stimulated the phaseollin biosynthetic pathway.

This effect contrasts with that reported for the elicitation of common bean with salicylic acid and derivatives, and isonicotinic acid and derivatives, in which the levels of coumestrol are similar or slightly higher than phaseollin.[9] Another noteworthy fact is that no necrosis of the root tissues was observed at the highest concentration tested, contrasting with previous biotests performed with synthetic analogs in our laboratory.[18,19]

In common bean seedlings, methyl jasmonate at 1.0 mM and above has shown symptoms of phytotoxicity.

In general, all the heterocyclic analogs of JA-Ile exhibited higher water solubility, compared to methyl jasmonate. The presence of the amino acid or its methyl ester, and the two nitrogen atoms in the cyclic system increase the polarity of the compounds and favoured the formation of hydrogen bonds with water. In addition, the aqueous solutions of pyrazolidin-3-ones did not emit strong or persistent odors. The fact that jasmonate-mediated responses are dependent on the configuration of the chiral carbons highlights the rarity of heterocyclic analogues displaying such strong phytoalexin-eliciting activity. This can be rationalized by considering that nitrogen atoms in cyclic systems can undergo pyramidal inversion, where the three groups connected to a nitrogen atom with a lone pair of electrons switch positions. This inversion affects the chirality of the molecule, causing it to become a mixture of stereoisomers. Thus, the use of pyrazolidine-3-ones as JA-Ile analogues could be an alternative to overcome the difficulties of jasmonates for field application, related to their low water solubility, high volatility, and strong odor. Additionally, the synthesis of pyrazolidine-3-ones is simpler and their amino acid conjugates are more readily available, given the complexities associated with the synthesis and purification of the active configuration of jasmonates.

2.2 Structure activity relationship (SAR)

The structural variations in the tested compounds and the results of the elicitor effect of phytoalexins allowed the establishment of some relationships, also summarized in Fig. 4.

Table 1 Results of the model quality assessment using ProSA-Web and PROCHECK

		Ramachandran plot				*G*-Factors				
Protein	Seq. identity	Core%	Allowed%	Generally allowed%	Disallowed%	Dihedrals	Covalent	Overall	*Z*-Score	Mean square
COI1_ARATH	100.0	80.0	19.2	0.80	0.00	−0.41	0.47	−0.07	−8.54	0.000
V7CZF7_PHAVU_SM	68.9	86.2	13.3	0.40	0.20	−0.35	−0.01	−0.20	−8.69	0.042
V7CZF7_PHAVU_IT	68.9	73.7	23.6	1.90	0.80	−0.75	−0.05	−0.45	−8.50	0.071
V7CZF7_PHAVU_AF	68.9	89.4	10.4	0.20	0.00	−0.11	0.30	0.06	−9.26	0.085
V7BBE9_PHAVU_SM	70.7	86.2	13.4	0.40	0.00	−0.36	−0.01	−0.21	−8.90	0.053
V7BBE9_PHAVU_IT	70.7	75.7	20.8	1.90	1.50	−0.66	−0.04	−0.39	−8.10	0.079
V7BBE9_PHAVU_AF	70.7	88.9	10.7	0.40	0.00	−0.12	0.30	0.06	−9.25	0.082

Table 2 Description of the amino acid residues in the pockets of the different models of the two orthologs

COI1 ARAT crystal	V7CZF7 PHAVU SM	V7CZF7 PHAVU AF	V7CZF7 PHAVU IT	V7BBE9 PHAVU SM	V7BBE9 PHAVU AF	V7BBE9 PHAVU IT
R85	R81	R81	R81	R76	R76	R76
A86	A82	A82	A82	A77	A77	A77
F89	F85	F85	F85	F80	F80	F80
L91	L87	L87	L87	L82	L82	L82
R348	R341	R341	—	R336	R336	—
E350	E343	E343	—	E338	E338	E338
A384	A377	A377	A377	A372	A372	A372
V385	V378	V378	V378	V373	V373	V373
Y386	Y379	Y379	Y379	Y374	Y374	—
R409	R402	R402	R402	R397	R397	R397
V411	V404	V404	V404	V399	V399	V399
Y444	Y437	Y437	Y437	Y432	—	Y432
L469	L462	L462	L462	L457	L457	L457
R496	R489	R489	R489	R484	R484	R484
W519	W513	W513	W513	W508	W508	W508

• From R^1: replacement of the pentenyl side chain by a saturated one only works while preserving the chain length.

• From R^1: in the case of saturated side chains, the shortening drops the activity more than the lengthening.

• From R^2: the change of the amino acid moiety did not alter the observed activity, at least for those tested with lipophilic side chain.

• From *n*: lengthening the linker between the ring and the amino acid makes the activity drop thoroughly.

• From R^3: protection of the carboxylic group of the amino acid portion is tolerated; however, such activity decreases *ca.* one-third of the corresponding free acid version.

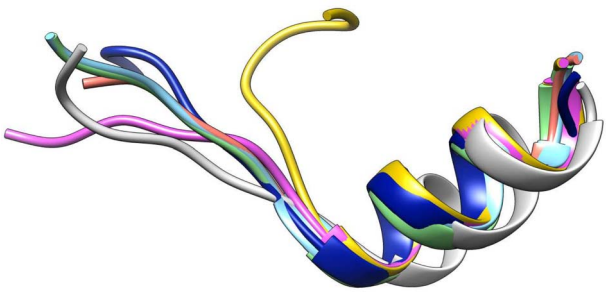

Fig. 5 Overlapping of the 3D degron structures. JAZ_degron_ARATH (light blue), V7AYI4_PHAVU_SM (green), V7AYI4_PHAVU_AF (pink), V7AYI4_PHAVU_IT (gray), V7CCD0_PHAVU_SM (orange), V7CCD0_PHAVU_AF (yellow).

2.3 Protein-complex receptor in *P. vulgaris*

The UniProt search based on the COI1 protein from *A. thaliana* (henceforth COI1_ARATH) yielded 240 hits, two of them from the species of interest with entry names V7CZF7_PHAVU and V7BBE9_PHAVU. The logo constructed with these protein sequences (see ESI†) shows high conservation between them, since the LRR motif, which allows the characteristic horseshoe conformation, is present in all of them.

The pdb file of COI1_ARATH has a small section without coordinates (R549-E563), which does not directly interfere with the ligand–protein or protein–protein interactions of the complex but matters to serve as a modeling template. To correct this, this random coil was modeled using the MODELLER tool of UCSF Chimera, choosing the one with the lowest zDOPE value (−1.27) that does not clash with the JAZ degron. Afterward, these two candidates were modeled using the three online tools, giving six models with the following code names: V7CZF7_PHAVU_SM, V7BBE9_PHAVU_SM, V7CZF7_PHAVU_IT, V7BBE9_PHAVU_IT, V7CZF7_PHAVU_AF and V7BBE9_PHAVU_AF. The values from the model quality assessment of the six proteins (Table 1) show that less than 2% of the residues are in disallowed regions according to the phi (ϕ) and psi (ψ) dihedral angles. In addition, *G*-factors from IT models are more negative than the others, by the higher percentage (0.80% and 1.50%) of residues in disallowed regions. Meanwhile, the models from AF had the highest *G*-factors, even more than the template protein used as a reference. However, the mean square shows how distant a model is to the reference, helping to choose the model that resembles the most COI_ARATH, in this case, V7CZF7_PHAVU_SM.

In addition to the quality values, the characterization of the amino acid residues within the pocket gave an impression of how similar this critical part is, compared to COI1_ARATH. In Table 2 there is a list of the residues within a sphere of 4.0 Å radius from the centroid of JA-Ile in the crystal. Here, the

Table 3 RMSD values from the comparison between the α-C of each degron model and the *A. thaliana* template

Degron model	RMSD [Å]
V7AYI4_PHAVU_AF	4.089
V7AYI4_PHAVU_IT	2.814
V7AYI4_PHAVU_SM	0.330
V7CCD0_PHAVU_AF	6.189
V7CCD0_PHAVU_IT	4.548
V7CCD0_PHAVU_SM	3.820

absence of one or more residues makes a difference that can be crucial for the binding energy measurements and, thereby can be a criterion for discarding a model. Thus, among the surviving models V7CZF7_PHAVU_SM was chosen, considering the similitude with COI1_ARATH observed for the quality assessment values.

For JAZ protein, the BLASTP found many orthologs of TI10A_ARATH, two for *P. vulgaris* with entry names V7AYI4_PHAVU and V7CCD0_PHAVU. The logo made for 20 of them (see ESI†) also depicts a highly conserved sequence, particularly in the region labeled as Jas motif. The template from *A. thaliana* only contains the degron, thus the orthologs in *P. vulgaris* were shortened as well, ensuring the inclusion of the Jas motif in all of them. Each model built for the two proteins was labeled with a suffix according to the tool used, namely _SM, _AF, or _IT. The N-terminus of the JAZ degron breaks the helical conformation between E200 and R206 to become stretched. Sheard *et al.* pointed out the importance of this portion for the ligand–protein interaction, consequently, refinements of the JAZ degrons of the PHAVU models were performed with MODELLER tool to fit such a conformation.[20] Fig. 5 shows an overlapping of the best outcome from MODELLER for each protein model, and Table 3 summarizes the Root Mean Square Deviation (RMSD [Å] eqn (1)) calculated between the α-C of each model compared with the template.

$$\mathrm{RMSD} = \sqrt{\frac{1}{n}\sum_{i=1}^{n} d_i^2} \quad (1)$$

From this information, V7AYI4_PHAVU_SM stands out as the best model for the JAZ degron, and along with V7CZF7_PHAVU_SM allowed the construction of the homologous protein-complex receptor model in *P. vulgaris* (Fig. 6). Both proteins were combined in a single pdb file, and the coordinate system was taken from the template, for simplicity of further calculations.

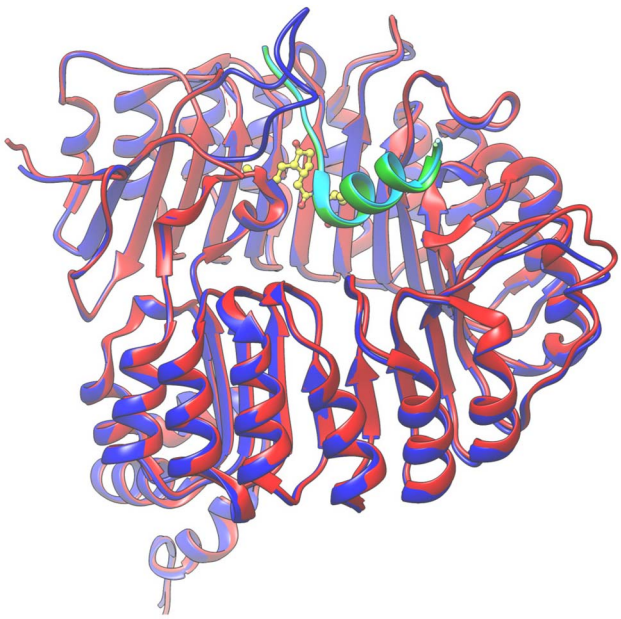

Fig. 6 Overlapping of the 3D structures of both models interacting with 9 (yellow) in the pocket. COI1_ARATH (red), JAZ_degron_ARATH (light blue), V7CZF7_PHAVU_SM (blue) and V7AYI4_PHAVU_SM (green).

Table 4 Conditions for the validation of the docking protocol *via* redocking

Entry	Ligand	Conformation	Rounds	Box size [Å^3]	Exhaustiveness
1	**9**	From crystal	20	30 × 30 × 30	32
2	**9**	From crystal	20	Auto	32
3	**9**	PM6 opt.	20	30 × 30 × 30	32
4	**9**	PM6 opt.	20	Auto	32
5	**8**	From crystal	20	30 × 30 × 30	32
6	**8**	From crystal	20	Auto	32
7	**8**	PM6 opt.	20	30 × 30 × 30	32
8	**8**	PM6 opt.	20	Auto	32

2.4 Docking validation

Some redocking experiments were performed to test the ability of the built model to reproduce the pose of the natural ligands **8** and **9** in the co-crystallized protein–ligand complex. The center of the box was set as the *centroid* of the corresponding natural ligand (x = 0.199783, y = 4.377261 and z = 47.645130). The results were analyzed regarding RMSD, which measures the deviation of the superimposed atomic coordinates from each pose and those from the corresponding ligand in the crystal. The results were compared regarding the binding energies [kcal mol^{-1}] and data dispersion to have an impression of expected values from a good hit. The conditions for the redocking are listed in Table 4.

The results after redock **8** and **9** in the COI1-JAZ_degron complex are shown in Fig. 7.

Here, the differences between the binding energy of both ligands reflect the widely observed fact that the phytotoxin **8** is more active than the native ligand **9**. Regardless of taking the same conformation as in the crystallized ligands (entries 1, 2, 5, and 6), RMSD values were *ca.* 0.5 Å higher than those for the previously optimized geometries with the PM6 basis set. Furthermore, experiments with box size automation (even entries) showed more negative binding energies and some with

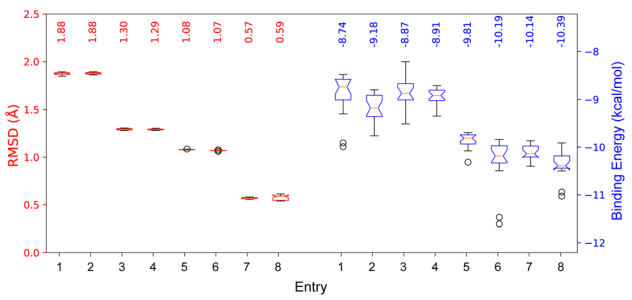

Fig. 7 RMSD and binding energies from redocking the native ligands **8** and **9** in the COI1-JAZ_degron protein complex.

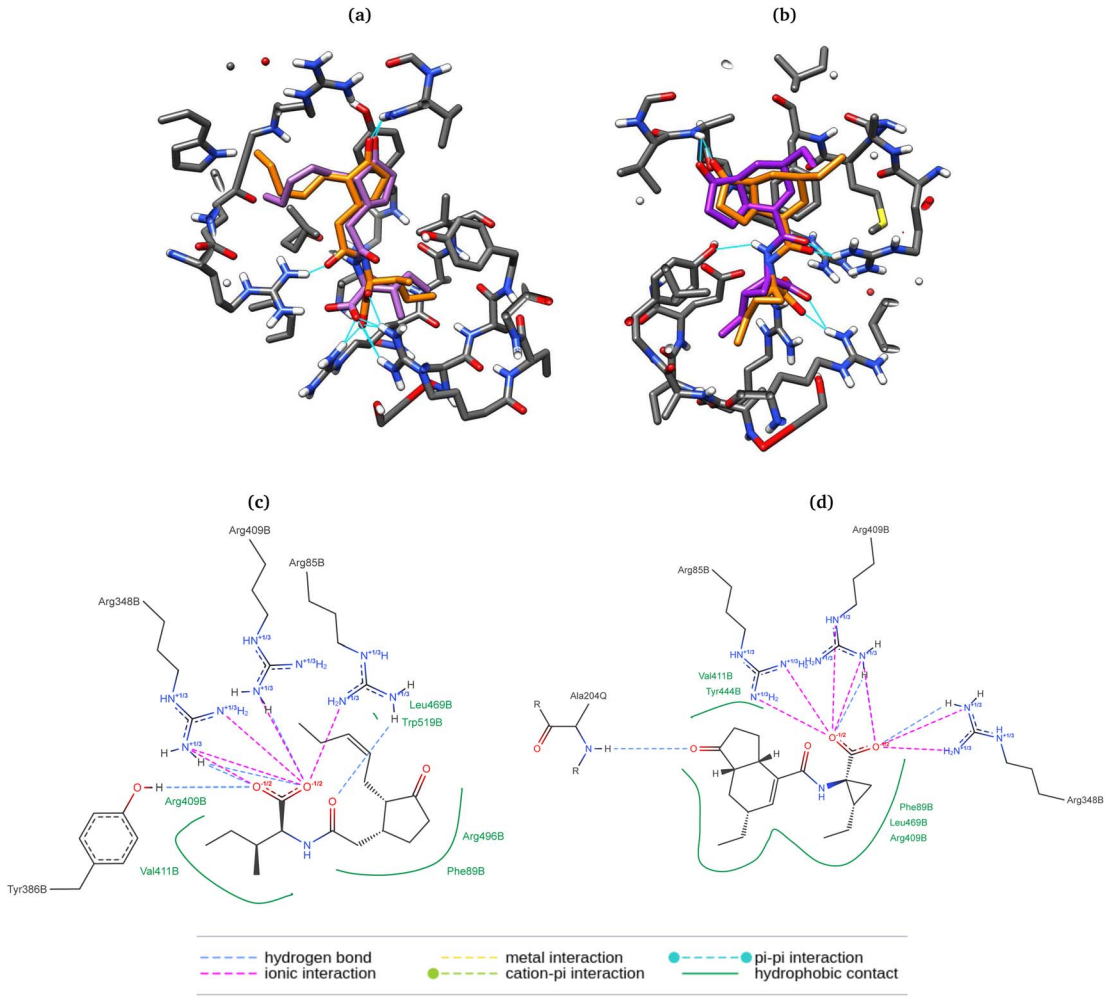

Fig. 8 3D representation of the poses of the natural ligands **9** (a) and **8** (b) from crystal (orange) and redocking (purple). Amino acids are represented in gray, and H-bonds in cyan. 2D description of interaction descriptions in the pocket for **9** (c) and **8** (d).

less data dispersion. Another interesting observation is that the RMSD is directly affected by the number of rotating bonds of the structure since the partial rigidity of the rings of **8** allows to get poses in the pocket close to the one in the crystal. All RMSD values were below the accepted threshold of 2.0 Å, and the best results (entries 4 and 8) were obtained when the

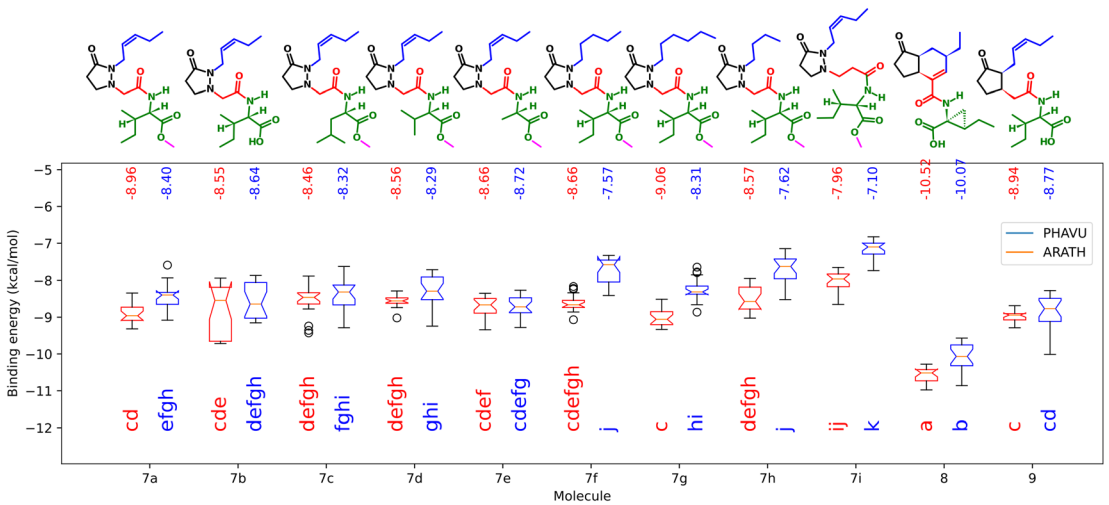

Fig. 9 Binding energies from the synthesized molecules docked in the protein models from *A. thaliana* (blue) and *P. vulgaris* (red). Boxes sharing the same letters have no significant differences.

geometry was previously optimized, and the box size automated. 2D depictions of the best poses for **8** and **9** (Fig. 8) have a planar representation of the hydrogen bonds between the carboxylic groups and the arginines 85, 348, 409, as well as the hydrophobic contact of the amino acid residues, the side chain and the ring with F89, R409, V411, Y444, L469, R496, W519. The key interaction between the carbonyl group of **8** and A204 from JAZ degron is also present. The mentioned conditions were implemented for the screening with both *A. thaliana* and *P. vulgaris* receptor models. 3D overlapped representations of redocking (Fig. 8) show how close the coordinates are from the crystallized natural ligands (orange) to those of the poses achieved from redocking (purple). H-bond interactions (cyan solid lines) with amino acid residues of the pocked are also depicted.

2.5 Docking

The binding energies form the docking of the synthesized molecules and the natural ligands in both receptors are plotted in Fig. 9.

Here, as expected, the more negative values correspond to **8**, having significant differences with **9**. As observed in the biological test, performance of the analogs did not change significantly when the amino acid residue was changed. For the free acid **7b**, lower energy values were achieved in the case of ARATH, but the data were more dispersed for both receptors, with no significant differences with the corresponding ester **7a**. On the other hand, results for **7i** also correspond to the observed in the biotest, suggesting that the lengthening of the linker disfavors the protein–ligand interactions in the pocket of the *P. vulgaris* receptor, releasing only −7.1 kcal mol^{-1}. In addition, the replacement of the side chain by a saturated one did not imply major changes in binding energies, according to the results in both receptors. The lower activity of compound **7h** was better represented by the results from PHAVU receptor, with a behavior similar to that in the bio-assay, the shorter the chain, the worse the activity.

A remarkable fact is that all tested molecules showed similar performances in both receptors, with a Pearson's coefficient of 0.722 (see ESI†). An overlapped 3D representation of the best poses of all molecules (Fig. 10) allows us to appreciate the key H-

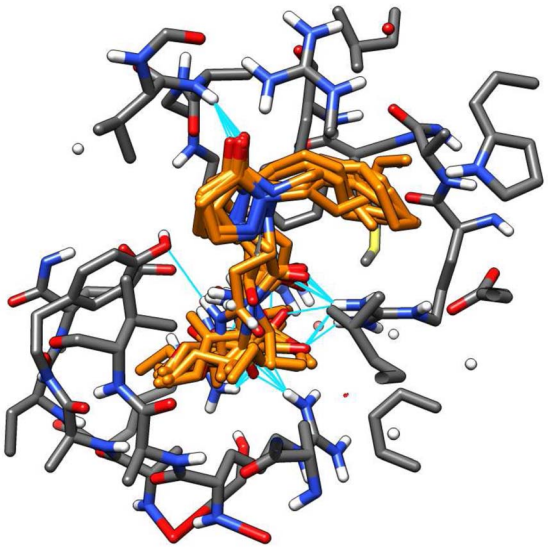

Fig. 10 3D overlapped representation of the best poses from the docking of all molecules.

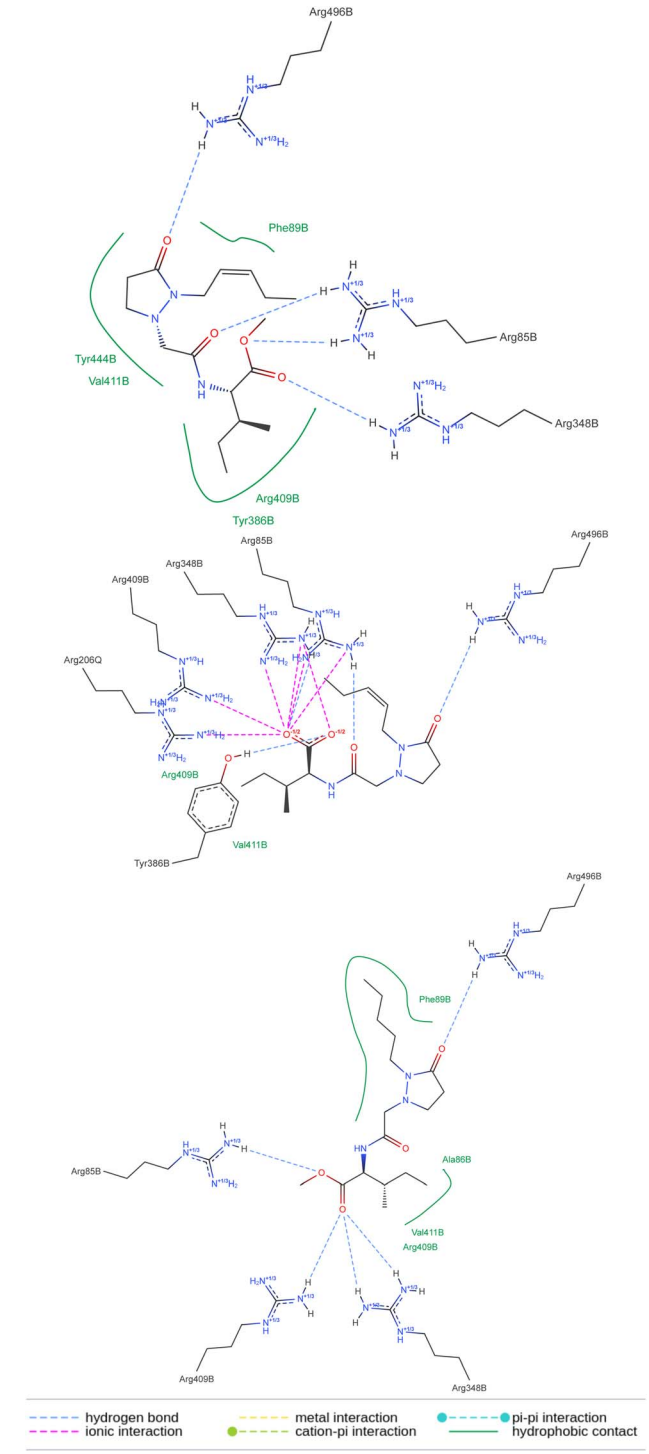

Fig. 11 2D representation of the best pose from the docking.

bond between the pyrazolidin-3-one carbonyl and the amide of the alanine residue in JAZ degron.

The above means that the protein receptor modeled for *P. vulgaris* is suitable for estimating the possible interactions if potential ligands reach the pocket of this target. The 2D representation of the docked molecules (Fig. 11) shows both sets of interactions in the active site of the protein complex, the hydrogen bonds between the carbonyls and the group of arginines, and the lipophilic contact between the bunch of methylenes in each molecule and the less polar amino acid residues. Despite the number of polar interactions being heigher for the free acid, they are not absent in the ester groups, which may justify the tolerance of this protecting group in the active site. To the best of our knowledge, the 3D structure of the protein-complex receptor in *P. vulgaris* is not known. It was obtained by homology modeling of the best hits from the search of orthologs of COI1 in *P. vulgaris*, using as a template the two co-crystalized structures available in the Protein Data Bank (PDB codes: 3ogk and 3ogl) for *A. thaliana*. The 3D models built were then used to have insight of the molecular interactions between these proteins and the tested ligands (JA-Ile, COR, and the pyrazolidin-3-one analogs) by the docking approach. Homology modeling using COI1-JAZ co-receptor has been used for different plant species.[22–24] Our results may be helpful for further experimental studies on promising scaffolds for the development of more specific elicitors, capable of triggering the chemical defense machinery of plants without detrimental consequences for their growth.

3 Conclusions

Nine synthetic jasmonoyl-L-isoleucine hetero-analogs were tested as elicitors of phytoalexin production in *P. vulgaris*. Most of the tested molecules elicited selective production of the bioactive metabolite phaseollin when added exogenously, even at a low concentration of 0.05 mM. The active molecules showed a dose-dependent behavior, and the structural differences between them allowed to establish tolerable changes such as the saturation or the elongation of the side chain, or exchange of the amino acid moiety as long as it remains lipophilic; While other changes dropped the activity, such as side chain shortening or linker elongation. The molecular receptor of jasmonate-like molecules was modeled by homology for *P. vulgaris* using the one of *A. thaliana* as a template. After assessing the built model, a docking screening of the tested molecules showed similar behavior for vina scores regarding the observed activity in the biological model. The 3D model of the protein-complex receptor in *P. vulgaris* provides novel insight into the molecular interactions among JA-Ile receptor, COR, and a series of pyrazolidin-3-ones that displayed phytoalexin-eliciting activity. Further studies should focus on determining the phytoalexin-eliciting potential of JA-Ile pyrazolidin-like analogs in other agriculturally important species, evaluating the effects of elicitor concentration, application time, phytotoxicity, improved resistance, among others. Furthermore, the findings reported in this article open the possibility for other heterocyclic nuclei to be considered in developing new synthetic elicitors for agriculture.

4 Experimental

4.1 General

Previous work describes the synthesis of pyrazolidine-like analogs of jasmonoyl-L-isoleucine.[25] Reagent-grade methyl jasmonate (**6**) and the standard-grade isoflavones daidzein (**2**) and genistein (**3**) were purchased in Sigma-Aldrich. The purification and characterization of coumestrol (**4**) and phaseollin (**5**) were described in a previous work.[15] HPLC-grade solvents were used for chromatography runs and sample preparation. The solutions of the potential elicitors were prepared with purified type II water and bidistilled commercial ethanol. Qualitative filter paper and PTFE 0.22 μm microfilters were used to filtrate the extracts and the HPLC samples, respectively. Seeds of *Phaseolus vulgaris* L. ICA Quimbaya variety were provided by Semillas el bosque S.A.S. High-Performance Liquid Chromatograph (HPLC) Hitachi Chromaster with a Diode Array Detector (DAD) was used for liquid chromatography. 3D protein and ligand visualizations were done in UCSF Chimera v 1.15 (**https://www.cgl.ucsf.edu/chimera/**).[26] The search for the orthologs of each protein was performed in the UniProt (**https://www.uniprot.org/**) database, while Clustal Omega (**https://www.ebi.ac.uk/jdispatcher/**) was the tool for multiple alignments. For protein modeling, SWISS-MODEL (**https://swissmodel.expasy.org/**) (SM), I-TASSER (**https://zhanggroup.org/I-TASSER/**) (IT), and AlphaFold (**https://alphafold.ebi.ac.uk/**) (AF) servers were chosen. The protein refinement was performed with the MODELLER (**https://salilab.org/modeller/**) tool inside UCSF Chimera software. The numerical values for the assessment of the models were obtained from the ProSA-web[27] (**https://prosa.services.came.sbg.ac.at/prosa.php**) and the SAVES v6.0 (**https://saves.mbi.ucla.edu/**) servers. All docking calculations were performed in Autodock Vina v1.2.3 and the 2D diagram of the ligand–protein interactions was modeled using the PoseView (**https://www.zbh.uni-hamburg.de/en/forschung/amd/server/poseview.html**) online free tool.[28] A list with the names, descriptions, and references is available online (**https://www.rdkit.org/docs/GettingStartedInPython.html**). Logos from the protein sequence alignments were performed with the WebLogo 3 (**https://weblogo.threeplusone.com/create.cgi**) online tool. For the ligand preparation, including input of the molecules and conversion to Mol2 and pdbqt formats, the RDKit (**https://www.rdkit.org/**) cheminformatics tool was used, along with Open Babel (**https://openbabel.org/**) the API toolkit.

4.2 Biological activity on bean cultivars

A specific variety of beans was chosen to evaluate the capacity of the synthesized analogs to trigger a chemical response through phytoalexin production. The ICA Quimbaya (aka red quartz) is recognized as an anthracnose-resistant variety, a property linked

to the quality of having the biochemical machinery to produce isoflavonoid phytoalexins with proven antimicrobial and antifungal activities.

4.2.1 Cultivation. The seeds were firstly washed four times with tap water, and the substrate (quartz sand) was disinfected with 1% aq. NaClO. The sowing was made in a rectangular array keeping a distance of 10 cm at least between each hole, watered daily, and kept in the dark at room temperature (r.t.). The sprouted seeds were employed for the elicitation test on the sixth day of cultivation.‡

4.2.2 Elicitation. The evaluation of the potential inductors was made at two levels, using solutions at 0.5 mM and 0.05 mM in 0.5% aq. EtOH.‡ The seedlings (with similar weights, heights or age) were carefully uprooted, rinsed with tap water, put in plastic cups, and randomly gathered in groups of 9 for each treatment. 10 mL of the corresponding treatment were added to each of the nine cups, ensuring the roots were immersed thoroughly in the solution. The induction process was made for two hours,‡ still in the dark, to prevent chlorophyll formation. Afterward, each solution of the inductors was poured out and replaced with cotton to keep the roots moist during the 84 h‡ of the post-induction period. The seedlings were treated with the 0.5% EtOH aq. solution as a negative blank, and 0.5 mM MeJas was used as a reference treatment for a positive induction.

4.2.3 Plant processing. After the 84 h post-induction period, hypocotyls and roots of the seedlings were processed in subgroups of 3 to form one replica. In the first step, the metabolic processes of each subgroup of plants were quenched with liquid N_2, and the frozen material was ground in a mortar to reduce particle size. Then it was weighed to get the grams of fresh weight (g.f.w.) and extracted with EtOH (96%, 3 × 10 mL). These extractions were made with the help of 6 min of continuous sonication in an ultrasound bath at 30 °C and 80 Hz. Afterward, the ethanolic extracts were pooled and centrifuged for 15 min at 4000 rpm. The supernatant was filtered through Whatman™ Qualitative filter paper, and the pellets were rinsed with EtOH (96%, 3 × 10 mL). The extracts were concentrated at reduced pressure, weighed, and used to prepare the HPLC samples.

4.2.4 Sample preparation. Each extract was redissolved in MeOH (5.0 mL) and filtered through a 0.22 μm PTFE filter. Final HPLC samples were obtained after 1 : 1 dilution of each filtrated with MeOH.

4.2.5 Calibration curves. Standards and purified phytoalexins from *P. vulgaris* (**2**, **3**, **4** and **5**) were used to build calibration curves with concentrations between 200 and 20 μg mL^{-1}. Each molecule was quantified at its wavelength of maximum absorption (λ_{max}), 248 nm, 259 nm, 278 nm and 343 nm respectively (see ESI†).

4.2.6 Chromatography conditions. The column was a ZORBAX Eclipse XDB C-18, 4.6 × 150 mm, and particle size of 5 μm. The temperature of the oven was set to 30 °C, the volume of injection to 20 μL, and the elution gradient as described in Table 5.

‡ This value was selected according to previous studies in our group.

Table 5 Elution gradient for the chromatography

Time [min]	0.5% HOAc aq. [%]	MeOH [%]	Flow [mL min^{-1}]
Init.	90.0	10.0	0.7
20.0	40.0	60.0	0.7
25.0	00.0	100.0	0.7
30.0	00.0	100.0	0.7
33.0	90.0	10.0	0.7
35.0	90.0	10.0	0.7

4.3 Construction of a docking receptor

Examining the potential protein–ligand interactions between the synthesized compounds and the active site of the target in *P. vulgaris* requires a suitable receptor. However, there are no reports of the three-dimensional structure of this protein complex for this species. Notwithstanding, two co-crystallized structures are available in the Protein Data Bank (PDB) for *A. thaliana*. These are the COI1-ASK1-COR-JAZ1_degron (PDB code: 3ogk) and the COI1-ASK1-JA-Ile-JAZ1_degron (PDB code: 3ogl) complexes, with X-ray diffraction resolutions of 3.18 Å and 2.80 Å respectively. This protein complex served as a template for the construction of the homologous target in the species under study, following the workflow described in Fig. 12.

4.3.1 Search for orthologs. To find the corresponding orthologs of the two proteins that directly interacts with the ligand, a BLASTP was performed in the UniPort database for both, COI1_ARATH and TI10A_ARATH. Default parameters such as the auto-BLOSUM62 matrix or the E-threshold of 10 were used.

4.3.2 Construction of the sequence logos. 20 of the hits found in the BLASTP were used to perform a multiple sequence alignment, including the two orthologs for each protein in *P. vulgaris*. The outcome from these alignments served as supplies for the construction of the logos, which illustrate the sequence conservation in each protein.

4.3.3 Building of the 3D protein model. 3D models of the best hits from the orthologs in *P. vulgaris* of both COI1_ARATH and TI10A_ARATH were built using COI1_ARATH and JAZ1_-degron as homologous templates in the SWISS-MODEL and I-

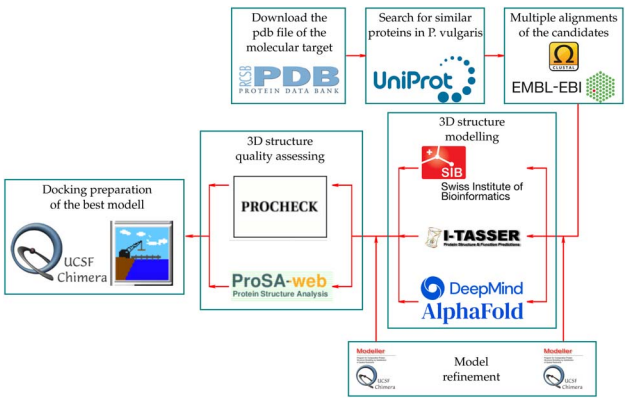

Fig. 12 Workflow for the construction of the protein target in *P. vulgaris*.

TASSER online tools, while AlphaFold already had them available.

4.3.4 Assessing of the models. The resulting models were assessed and compared to the templates regarding their Ramachandran plot values, *G*-factors, *Z*-score, and sequence identity. In addition, the amino acid residues within a sphere with a radius of 4.0 Å from the centroid of JA-Ile were listed.

4.4 Docking experiments

4.4.1 Ligand and receptor preparation. The receptor preparation was performed with the DockPrep tool of UCSF Chimera for all the docking experiments. This protocol includes a solvent and complexed ions deletion, incomplete side chains replacement with Dynamemonics Rotamers Library, addition of hydrogens and charges (AMBER ff14SB, Gasteiger), and conversion to a Mol2 file before the final pdbqt input of the vina software.

The ligand preparation also included the addition of hydrogens and charges and conversion to the pdbqt inputs *via* the Mol2 file. However, Open Babel software was used in this case.

4.4.2 Parameters and conditions. All the docking process, from the smiles inputs to the resulting plots was automated in customized software. Molecules to be docked were previously geometrically optimized using a PM6 basis set. Docking experiments were performed 20 times for each molecule with exhaustiveness of the search set to 32, using the centroid of the co-crystallized ligand **9** as the center of coordinates, and with a box size automatically set for each ligand. Box size automation was implemented in the custom software following the procedure described by Feinstein *et al.*[29] In such a study, the highest prediction accuracy in vina docking was achieved when the ratio between the Radius of Gyration (R_g) and the box size was 0.35, which is, $2.857 \times R_g$. This value was calculated according to eqn (2) for a single conformer due to its correlation with the average value for a hundred conformers. N is the total number of heavy atoms, $\vec{r}_k$ corresponds to the cartesian coordinates of each heavy atom, and $\vec{r}_{\text{center}}$ are the coordinates of the centroid of the ligand.

$$R_g = \sqrt{\frac{1}{N}\sum_{k=1}^{N} |\vec{r}_k - \vec{r}_{\text{center}}|^2} \quad (2)$$

4.4.3 Comparison of means. A pairwise comparison between the means of all treatments was performed by a *post hoc* Tukey's honestly significant difference (HSD) test, with a confidence interval of 0.95. The SciPy algorithm for this statistical comparison was implemented in a Jupyter notebook.

Data availability

The data supporting this article have been included as part of the ESI.† Source code of the software for docking automation and data processing is part of an ongoing personal, non-profit project, and it can be found here (**https://github.com/samuelvp360/SVP360CalculationController/tree/new_version**) with DOI: **https://doi.org/10.5281/zenodo.13698825**. The version of the code employed for this study is version 1.0. The data analysis script to plot the results with the Tukey test for the inductions is available in the interactive notebook Google Collab here (**https://colab.research.google.com/drive/1DwaLIqt8J-pQjs8zquOKyTtSBsD5VSol?usp=sharing**). The data analysis script to plot the results from docking is available here (**https://colab.research.google.com/drive/1FFWQhORWVdZHdYb07raLdisMhgvSXq7x?usp=sharing**). To reproduce the plots in both cases, first open the Collab session, upload the corresponding raw csv data provided in the ESI,† then run all cells.

Author contributions

Concept: W. Q. F., and D. D.; experiments: S. V. P.; supervision and resources: D. D. and W. Q. F.; writing: S. V. P., D. D. and W. Q. F.

Conflicts of interest

There are no conflicts to declare.

Acknowledgements

The authors thanks Minciencias (Ministerio de Ciencia Tecnología e Innovación de Colombia) for financial support (Grant No. 111874558342; FP44842-057-2017).

Notes and references

1 S. Fonseca, A. Chini, M. Hamberg, B. Adie, A. Porzel, R. Kramell, O. Miersch, C. Wasternack and R. Solano, *Nat. Chem. Biol.*, 2009, **5**, 344–350.
2 M. Reyes-Díaz, T. Lobos, L. Cardemil, A. Nunes-Nesi, J. Retamales, M. Alberdi and A. Ribera-Fonseca, *Molecules*, 2016, **21**(6), 567.
3 G. Haider, T. von Schrader, M. Füßlein, S. Blechert and T. M. Kutchan, *Biol. Chem.*, 2000, **381**, 741.
4 U. Hartmond, R. Yuan, J. K. Burns, A. Grant and W. J. Kender, *J. Am. Soc. Hortic. Sci.*, 2000, **125**(5), 547–552.
5 L. Holbrook, P. Tung, K. Ward, D. M. Reid, S. Abrams, N. Lamb, J. W. Quail and M. M. Moloney, *Plant Physiol.*, 1997, **114**, 419–428.
6 G. Flores, G. P. Blanch and M. L. Ruiz del Castillo, *Food Chem.*, 2013, **141**, 2982–2987.
7 K. Müller and H. Börger, *Experimentelle Untersuchungen über die Phytophthora – Resistenz der Kartoffel*, 1939.
8 H. D. VanEtten, J. W. Mansfield, J. A. Bailey and E. E. Farmer, *Plant Cell*, 1994, **6**, 1191–1192.
9 D. Durango, N. Pulgarin, F. Echeverri, G. Escobar and W. Quiñones, *Molecules*, 2013, **18**, 10609–10628.
10 L. D. Cox, S. Munholland, L. Mats, H. Zhu, W. L. Crosby, L. Lukens, K. P. Pauls and G. G. Bozzo, *Metabolites*, 2021, **11**, 1–25.
11 D. A. Smith, H. D. Van Etten and D. F. Bateman, *Physiol. Plant Pathol.*, 1975, **5**, 51–64.

12 H. D. VanEtten and D. F. Bateman, *Phytopathology*, 1971, **61**, 1363–1372.
13 F. Redko, M. L. Clavin, D. Weber, F. Ranea, T. Anke and V. Martino, *Z. Naturforsch. C*, 2007, **62**, 164–168.
14 F. Zhang and D. L. Smith, *J. Exp. Bot.*, 1996, **47**, 785–792.
15 D. Durango, W. Quiñones, F. Torres, Y. Rosero, J. Gil and F. Echeverri, *Molecules*, 2002, **7**, 817.
16 L. Botero, S. Vizcaíno, W. Quiñones, F. Echeverri, J. Gil and D. Durango, *Biotechnol. Rep.*, 2021, **29**, e00601.
17 D. Aristizábal, J. Gil, W. Quiñones and D. Durango, *Molecules*, 2022, **27**, 3500.
18 F. E. Quenguan, Derivados del acido 1-oxo-4-indanoil carboxílico como potenciales elicitores de defensas química en leguminosas cultivadas en Colombia., 2020, available at **https://repositorio.unal.edu.co/handle/unal/80087**.
19 K. Gómez, F. Quenguan, D. Aristizabal, G. Escobar, W. Quiñones, O. García-Beltrán and D. Durango, *Heliyon*, 2022, **8**, e08979.
20 L. B. Sheard, X. Tan, H. Mao, J. Withers, G. Ben-Nissan, T. R. Hinds, Y. Kobayashi, F.-F. Hsu, M. Sharon, J. Browse, S. Y. He, J. Rizo, G. A. Howe and N. Zheng, *Nature*, 2010, **468**, 400.
21 J. Yan, C. Zhang, M. Gu, Z. Bai, W. Zhang, T. Qi, Z. Cheng, W. Peng, H. Luo, F. Nan, Z. Wang and D. Xie, *The Plant Cell*, 2009, **21**, 2220–2236.
22 F. Valenzuela-Riffo, A. Garrido-Bigotes, P. M. Figueroa, L. Morales-Quintana and C. R. Figueroa, *J. Mol. Graphics Modell.*, 2018, **85**, 250–261.
23 I. Monte, J. Caballero, A. M. Zamarreño, G. Fernández-Barbero, J. M. García-Mina and R. Solano, *Proc. Natl. Acad. Sci. U. S. A.*, 2022, **119**, e2212155119.
24 Y. Nakamura, C. Paetz, W. Brandt, A. David, M. Rendón-Anaya, A. Herrera-Estrella, A. Mithöfer and W. Boland, *J. Chem. Ecol.*, 2014, **40**, 687–699.
25 S. Vizcaíno Páez, D. Durango, C. J. Müller, M. Breuning and W. Quiñones Fletcher, *RSC Adv.*, 2024, **4**, 3790–3797.
26 E. F. Pettersen, T. D. Goddard, C. C. Huang, G. S. Couch, D. M. Greenblatt, E. C. Meng and T. E. Ferrin, *J. Comput. Chem.*, 2004, **25**, 1605–1612.
27 M. J. Sippl, *Proteins: Struct., Funct., Bioinf.*, 1993, **17**, 355–362.
28 K. Stierand and M. Rarey, *ACS Med. Chem. Lett.*, 2010, **1**, 540–545.
29 W. P. Feinstein and M. Brylinski, *J. Cheminf.*, 2015, **7**, 18.